resolution than has been attempted to date.

Our new findings still leave unexplained the Dansgaard–Oeschger oscillations in air temperature over Greenland that punctuate the intervals between the Heinrich events. Perhaps, as we suggested earlier[3], these reflect the salt-induced ocean circulation oscillations caused by an interaction between the ocean heat-pump and the Scandinavian ice sheets. Although many questions remain unanswered, our correlation of the Heinrich events so prominent in the ice cores with the more frequent Dansgaard-Oeschger events in the ice cores brings us significantly closer to understanding the complex link between ice-sheet dynamics and ocean operation. □

Received 21 April; accepted 16 July 1993.

1. Dansgaard, W. *et al. Nature* **364,** 218–220 (1993).
2. Broecker, W. S. *et al. Quat. Res.* **30,** 1–6 (1988).
3. Broecker, W. S., Bond, G. & Klas, M. *Paleoceanogr.* **5(4),** 469–477 (1990).
4. Bond, G. *et al. Nature* **360,** 245–249 (1992).
5. Broecker, W. S., Bond, G., Klas, M., Clark, E. & McManus, J. *Clim. Dynamics* **6,** 265–273 (1992).
6. Bé, A. W. H. & Tolderlund, D. S. *Micropaleontology of Oceans* (eds Funnell, B. M. & Riedel, W. R.) 105–149 (Cambridge Univ. Press, 1971).
7. Kellogg, T. B. *Boreas* **9,** 115–137 (1980).
8. Broecker, W. S. *Paleoceanogr.* **3(1),** 1–19 (1988).
9. Lehman, S. J. & Keigwin, L. D. *Nature* **356,** 757–762 (1992).
10. Karpuz, N. C. & Jansen, E. *Paleoceanogr.* **7(4),** 499–520 (1992).
11. Bond, G., Broecker, W., Lotti, R. & McManus, J. in *Start of a Glacial* (eds Kukla, G. J. & Went, E.) 185–205 (Springer, Berlin, 1992).
12. Johnsen, S. J. *et al. Nature* **359,** 311–313 (1992).
13. Alley, R. B. *et al. Nature* **362,** 527–529 (1993).
14. Bard, E., Arnold, M., Fairbanks, R. G. & Hamelin, B. *Radiocarbon* **3(1),** 191–199 (1993).
15. Martinson, D. G. *et al. Quat. Res.* **27,** 1–29 (1987).
16. Dansgaard, W., White, J. W. C. & Johnsen, S. J. *Nature* **339,** 532–533 (1989).
17. Taylor, K. C. *et al. Nature* **361,** 432–436 (1993).
18. Heinrich, H. *Quat. Res.* **29,** 142–152 (1988).
19. Ruddiman, W. F. & McIntyre, A. *Paleogeogr. Palaeoclimatol. Palaeoecol.* **35,** 145–214 (1981).
20. Duplessy, J-C., Labeyrie, L., Juillet-LeClerc, A. & Duprat, J. in *The Last Deglaciation: Absolute and Radiocarbon Chronologies* (eds Bard, E. & Broecker, W. S.) 201–208 (Springer, Berlin, 1992).
21. Andrews, J. T., Tedesco, K., Briggs, W. M. & Evans, L. W. *Can. J. Earth Sci.* (in the press).
22. MacAyeal, D. R. *Nature* **359,** 29–32 (1992).
23. Ruddiman, W. F. in *Northern America and Adjacent Oceans during the Last Deglaciation: The Geology of North America* (eds Ruddiman, W. F. & Wright, H. E. Jr) 137–154 (Geol. Soc. of Am, Boulder, 1987).
24. Sancetta, C., Imbrie, J. & Kipp, N. G. *Quat. Res.* **3,** 110–116 (1973).
25. Woillard, G. & Mook, W. G. *Science* **215,** 159–161 (1982).
26. Shakleton, N. J., Imbrie, J. & Hall, M. A. *Earth planet. Sci. Lett.* **65,** 233–244 (1983).
27. Bloom, A. L., Broecker, W. S., Chappell, J. M. A., Matthews, R. K. & Mesolella, K. J. *Quat. Res.* **4,** 185–205 (1974).

ACKNOWLEDGEMENTS. This research was supported in part by grants from the US National Science Foundation (NSF) and NOAA. The ice-core data are from the Greenland Ice Core Project (GRIP) organized by the European Science Foundation. The measurement of planktic $\delta^{18}O$ was supported by the French CNRS, CEA and CEE(EPOCH). We thank the Ocean Drilling Program for permission to sample cores from DSDP site 609. Support for the core collection of Lamont-Doherty Geological Observatory is provided by the NSF and the Office of Naval Research. We thank C. Sancetta for providing her unpublished diatom data from DSDP site 609. We also thank G. Denton, E. Jansen, S. Leyman, D. MacAyeal and P. Mayewski for comments on the manuscript.

Sharpness of upper-mantle discontinuities determined from high-frequency reflections

H. M. Benz* & J. E. Vidale†

* US Geological Survey, Golden, Colorado 80401, USA
† US Geological Survey, Menlo Park, California 94025, USA

AN understanding of the nature of seismic discontinuities in the Earth's upper mantle is important for understanding mantle processes: in particular, the amplitude and sharpness of these discontinuities are critical for assessing models of upper-mantle phase changes and chemical layering. So far, seismic studies aimed at determining the thickness and lateral variability of upper-mantle discontinuities have yielded equivocal results, particularly for the discontinuity at 410 km depth[1,2]. Here we present short-period (0.8–2.0 s) recordings of upper-mantle precursors to the seismic phase P′P′ (PKPPKP) from two South American earthquakes recorded by the ~700-station short-period array in California. Our results show that the 410- and 660-km discontinuities beneath the Indian Ocean are locally simple and sharp, corresponding to transition zones of 4 km or less. These observations pose problems for mineral physics models[3–5], which predict a transitional thickness greater than 6 km for the peridotite to β-spinel phase transition. In contrast to the results of long-period studies[6,7], we observe no short-period arrivals from near 520 km depth.

Experimental and thermodynamic studies[3–5,8] suggest that a peridotite to β-spinel phase transition near 410 km depth occurs over a range of 6–19 km, whereas a δ-spinel to perovskite and magnesiowüstite phase transition near 660 km depth occurs over a smaller range of 1–10 km. Some argue[9], on the basis of seismic observations of sharp discontinuities, that the upper mantle is chemically stratified, while others[10] propose a non-equilibrium phase transformation as a possible explanation for the observation of sharp boundaries. Topographic variations of ±20 km on the 660-km discontinuity[11] favour phase transitions. A recent seismic investigation[12] of near-receiver converted phases argues for a transitional 660-km discontinuity (20–30 km in thickness) and a sharp 410-km discontinuity. These results contradict previous studies of P′P′ precursors[1,13–15] that observed a simple and sharp 660-km discontinuity. A paucity of high-frequency P′P′ precursors from near 410 km depth[1,2,15] has made it difficult to determine the sharpness of this discontinuity. This leads some[2] to suspect defocusing effects due to topography or lateral variations in transitional thickness. Previous studies[1,2,15] have been limited in their ability to characterize the lateral variability in the sharpness of the 410-km discontinuity, primarily owing to small array apertures and sparseness of observations.

From our survey of large-magnitude South American earthquakes ($M > 6.2$), all clear P′P′ arrivals were accompanied by short-period (0.8–2.0 s) $P'_{660}P'$ precursors, implying that the 660-km discontinuity beneath the Indian Ocean is simple and sharp, consistent with previous P′P′ observations[1,13–15]. The dense sampling and large aperture of our array (Fig. 1*a*), combined with the two closely spaced South American earthquakes leads to unprecedented sampling of the upper mantle, enabling us to show the best evidence to date that the 410-km discontinuity is locally as sharp as 4 km thick, but varies laterally over distances of 250–500 km. This lateral variation may explain the paucity of observations and difficulty in measuring the impedance contrast and sharpness of this discontinuity[1,2,15].

Numerous investigations of the transitional upper mantle from 200 to 700 km depth have been made over the past fifty years. The thickness and relative velocity contrast of upper mantle discontinuities are best determined from wide-angle P and S waves[16–18] recorded in the distance range 15° to 30°, near-source[19,20] and near-receiver[12,21,22] reflections and conversions, or from PP, SS and P′P′ precursors[1,2,13–15,23–25].

P′P′ (PKPPKP), which is best observed in the distance range 65° to 75° with a caustic occurring near 71°, has been widely studied because its precursors (typically under-side reflections from mantle discontinuities) are ideal for identifying and measuring the transitional thickness of such discontinuities. P′P′ precursors are commonly labelled as P'_dP' where d denotes the depth of the reflector. We will use this convention, and will refer to the three main upper-mantle discontinuities by their average globally observed depths, that is, the 410-, 520- and 660-km discontinuities[7,11].

Since the early 1970s, the United States Geological Survey (USGS) and the California Institute of Technology have been operating regional seismic arrays in California (Fig. 1*a*). These

consist of 700 high-gain, short-period (1 Hz), vertical-component seismic stations that are ideal for recording low-amplitude, high-frequency P'P' precursors. The two South American events discussed here represent the best examples of P'P' and its upper mantle precursors recorded by this array since we began looking for P'P' phases in June 1990. The region of the mantle sampled by these earthquakes spans approximately 600–1,000 km beneath the Indian Ocean (Fig. 1*b*), with each event sampling a portion of the mantle 250 km apart.

Shown in Fig. 2 are the record sections of the P'P' window for two South American earthquakes recorded in California. The Peru–Brazil event was well-recorded at 140 stations (Fig. 2*a*), whereas the southern Peru earthquake was well-recorded on 231 stations (Fig. 2*b*). P'P' is observed in the period range 0.7–4.0 s, whereas the precursors are clearly observed between 1.0–2.0 s and weakly observable between 0.8–1.0 s. A dominant period of 1.5 s for the precursor is comparable to a dominant period of 1.2–3.0 s in previous studies[1,15]. Both profiles (Fig. 2) show clearly a $P'_{660}P'$ phase, while $P'_{410}P'$ is observed from only one event. From the Peru–Brazil earthquake (Fig. 2*a*), P'P' (2,275–2,290 s), $P'_{660}P'$ (2,140–2,160 s) and $P'_{410}P'$ (2,190–2,210 s) are observed from 64° to 71°. The southern Peru earthquake (Fig. 2*b*) produced P'P' (2,320–2,345 s) and $P'_{660}P'$ (2,180–2,210 s) from 68° to 75°. The $P'_{410}P'$ phase is most likely to be observed near its caustic, which is at about 72°, but the record section (Fig. 2*b*) shows no evidence for such a phase.

Estimates of the sharpness of the 410 and 660-km discontinuities can be determined from P'P' observations[15,26], but depths to the reflectors are difficult to ascertain. This is due to imprecise measurement of the arrival time and poorly known upper-mantle and crustal-velocity structure. A change of 10 km in the depth of the 660-km discontinuity produces a travel-time difference of ~2 s for the precursor, which is small given the uncertainties in the velocity structure. Comparing the observed data with theoretical arrival times using the IASP91 reference model[27], estimated reflector depths of the precursors are measurable to ±10 km. We find a depth of 650 km beneath the Indian Ocean, which is consistent with longer period estimates of <650 km for the same region[28].

Waveform similarity and a dominant period of 1.5 s for the $P'_{410}P'$ and $P'_{660}P'$ precursors (Fig. 3*a*) suggest that the 410- and 660-km discontinuities sampled by the Peru–Brazil earthquake are simple and sharp. One would expect to observe relative frequency and waveform differences for either a transitional discontinuity or topography on the discontinuity, neither of which are observed.

No evidence of a sharp seismic discontinuity (thickness <4 km) near 520 km depth is found in the stacked traces (Fig. 3*b*). The stacked record, aligned on $P'_{410}P'$, displays uniform coda levels in the time window appropriate for a precursor from

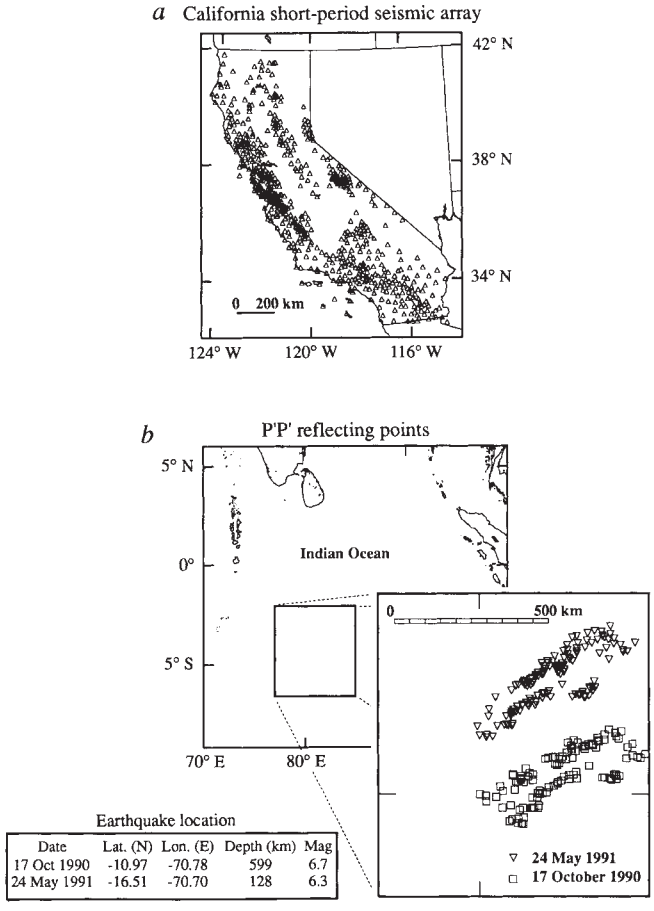

FIG. 1 *a*, Location of the approximately 700 short-period, vertical-component seismic stations (triangles) operated in California by the US Geological Survey and the California Institute of Technology. *b*, Location of the mid-point reflections of the P'P' phase from two South American earthquakes recorded by the California short-period seismic array.

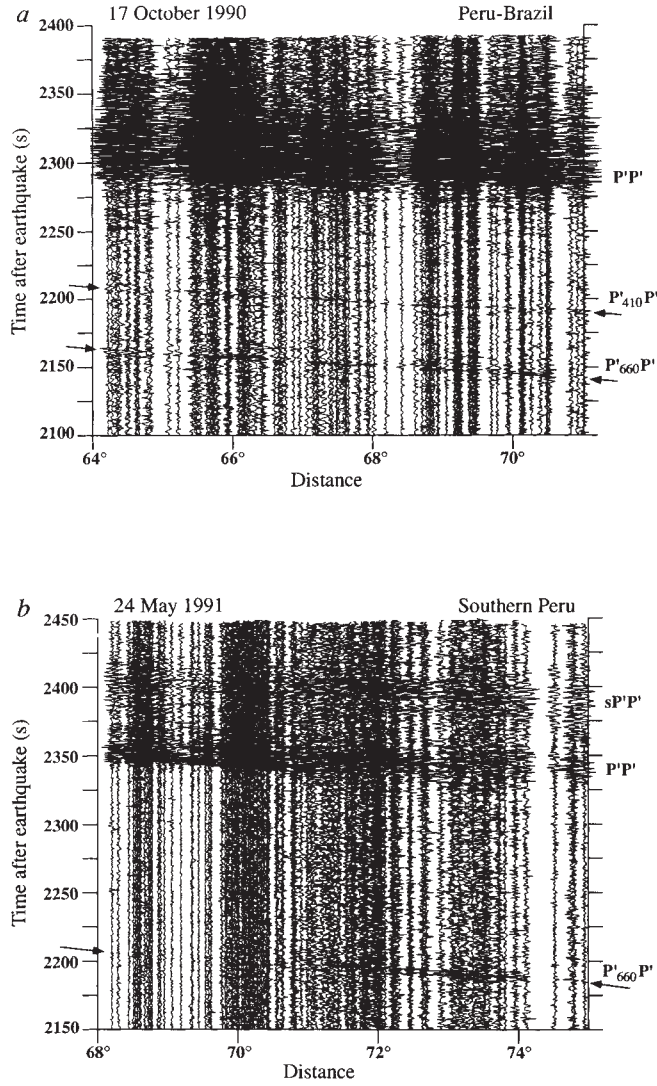

FIG. 2 P'P' record sections for two South American earthquakes recorded by the California seismic array. Each trace is normalized to a constant width, and only traces with a signal-to-noise ratio greater than 5 are shown.

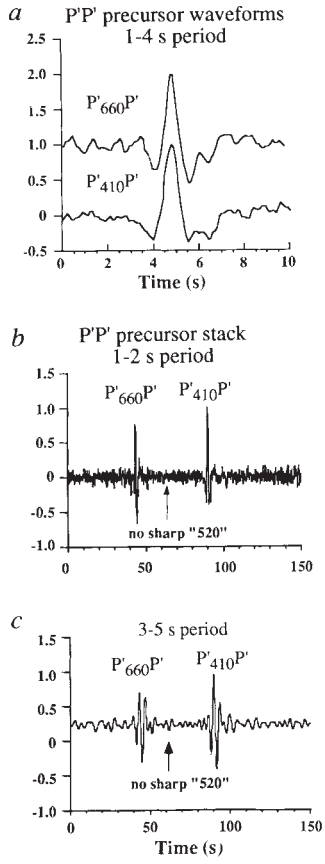

FIG. 3 *a*, Comparison of the precursor waveforms from stacking the 70 seismograms that recorded both $P'_{410}P'$ and $P'_{660}P'$ phases. Each seismic record was aligned on the appropriate precursor before summing. The similar frequency content and waveform shape for the two precursors argue for simple and sharp velocity discontinuities. The *y* axes in this figure represent normalized amplitude. *b*, Stack of upper-mantle precursors showing no high-frequency evidence for a precursor near 520 km depth. The stack was produced by aligning records on the $P'_{410}P'$ phase before summing. *c*, Low-frequency stack of upper-mantle precursors, demonstrating that the transitional thickness of a 520-km discontinuity must be greater than 10 km.

near 520 km depth. A low-frequency stack (Fig. 3*c*) also shows no evidence for a 520-km discontinuity, which implies that the transitional thickness of this discontinuity must be greater than 10 km. Lack of support for a sharp discontinuity near 520 km depth is consistent with wide-angle, short-period observations in Australia[29] and southern California[30].

Several studies of P'P' precursors[1,2,15] have noted the paucity of observations from near 410 km depth, which suggests that this boundary may be more complex and difficult to quantify in terms of its impedance contrast and transitional thickness. Factors that may explain these observations are lateral variations in the transitional thickness and impedance contrast of the discontinuity, or topographic relief along the boundary[2]. Synthetic seismogram simulations[2] show that topographical changes (with wavelengths and amplitudes of the order of 300 km and 10 km respectively) can decrease the amplitude of P'P' precursors by a factor of 2–4. Variations in the impedance contrast and transitional thickness of the discontinuity can decrease the amplitude of a precursor by similar or greater amounts[15,26]. Each is adequate to explain the lack of the $P'_{410}P'$ precursor for the southern Peru earthquake. Alternatively, focusing effects can increase the observed amplitude by a factor of 2–4, making it difficult to estimate the reflection coefficient at the boundary[3]. But the observed frequency content of the precursor provides excellent constraints on the maximum transitional thickness of the discontinuity.

We use reflectivity synthetic seismograms to determine the maximum transitional thickness consistent with the $P'_{410}P'$ precursor observed in the frequency range 0.5–1.0 Hz. Because it is difficult to determine an appropriate attenuation model beneath the Indian Ocean, relative amplitudes between P'P' and its precursors are difficult to compare. But the synthetic seismograms can be used to explain relative differences between $P'_{410}P'$ and $P'_{660}P'$, as attenuation between the two discontinuities is not appreciable.

Reflectivity synthetic seismograms for three velocity models (Fig. 4) were computed at frequencies of 0.5–1.0 Hz and a distance (δ) of 70.5°, where the amplitudes of the $P'_{410}P'$ and $P'_{660}P'$ are comparable and $P'_{410}P'$ is most likely to be observed. Synthetic seismograms show a 75% decrease in the $P'_{410}P'$ amplitude for a 4-km-thick transition zone and no observable $P'_{410}P'$ for a 6-km-thick transition zone, relative to a first-order

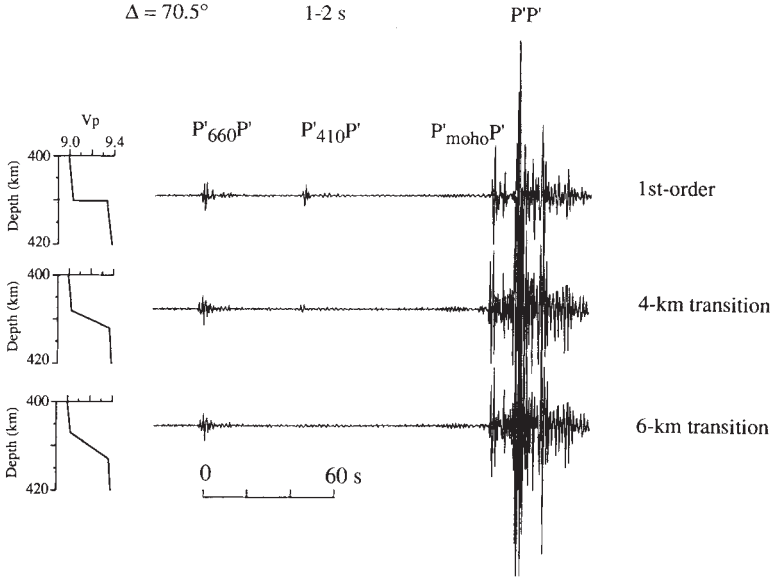

FIG. 4 Reflectivity synthetic seismograms of P'P' and its precursors for different thickness of the 410-km discontinuity and a constant distance (Δ) of 70.5°. For all three cases, a discontinuity at 660 km is modelled as a first-order discontinuity, while the 410-km discontinuity is modelled as 0, 4 and 6-km-thick transition zones. Seismograms were computed using the IASP91 velocity model[27] and the PREM density model[31]. Upper mantle low velocity zone densities were modified to be consistent with higher IASP91 velocities. Synthetic seismograms were computed in the frequency band 0.2–1.0 Hz with constant P- and S-wave quality factors of 5,000 and 2,000, respectively.

discontinuity. Synthetic seismograms demonstrate that a maximum transitional thickness of 4 km is necessary to generate the observed precursor. Since the amplitude of the reflection is falling off rapidly in the period range 1–2 s for a 4-km-thick transition, a maximum thickness of 2 km is likely. The results are consistent with theoretical reflection coefficient calculations[26] that estimate a 4-km-thick transition for 2 s periods and a thinner transition for shorter periods. Our data are not sufficient to rule out either topographic or transitional variations as the cause of the variability of $P'_{410}P'$ observations. But high-frequency observations and synthetic seismograms clearly show that the 410-km discontinuity is, at least locally, too sharp for its current phase boundary explanation. □

Received 9 March; accepted 9 July 1993.

1. Nakanishi, I. *Geophys. J.* **93,** 335–346 (1988).
2. Davis, J. P. *Geophys. J. Int.* **99,** 595–604 (1989).
3. Katsura, T. & Ito, E. *J. geophys. Res.* **94,** 15663–15670 (1989).
4. Akaogi, M., Ito, E. & Navrotsky, A. *J. geophys. Res.* **94,** 15671–15685 (1989).
5. Bina, C. R. & Wood, B. J. *J. geophys. Res.* **92,** 4853–4866 (1987).
6. Shearer, P. M. *Nature* **344,** 121–126 (1990).
7. Revenaugh, J. & Jordan, T. H. *J. geophys. Res.* **96,** 19763–19780 (1991).
8. Ito, E. & Takahashi, E. *J. geophys. Res.* **94,** 10637–10646 (1989).
9. Anderson, D. L. & Bass, J. D. *Nature* **320,** 321–328 (1986).
10. Solomatov, V. S. & Stevenson, D. J. *Nature* (submitted).
11. Shearer, P. M. & Masters, T. G. *Nature* **335,** 791–796 (1992).
12. Petersen, N. *et al. Geophys. Res. Lett.* **20,** 859–862 (1993).
13. Engdahl, E. R. & Flinn, E. A. *Science* **163,** 177–179 (1969).
14. Adams, R. D. *Bull. seism. Soc. Am.* **61,** 1441–1451 (1971).
15. Lees, A. C., Bukowinski, M. S. T. & Jeanloz, R. *J. geophys. Res.* **88,** 8145–8159 (1983).
16. Helmberger, D. V. & Wiggins, R. A. *J. geophys. Res.* **76,** 3229–3245 (1971).
17. Hales, A. L., Muirhead, K. J. & Rynn, J. M. W. *Tectonophysics* **63,** 309–348 (1980).
18. Grand, S. P. & Helmberger, D. V. *Geophys. J. R. Astr. Soc.* **76,** 399–438 (1984).
19. Richards, M. A. & Wicks, C. W. *Geophys. J. Int.* **101,** 1–35 (1990).
20. Vidale, J. E. & Benz, H. M. *Nature* **356,** 678–683 (1992).
21. Paulssen, H. *J. geophys. Res.* **93,** 10489–10500 (1988).
22. Bock, G. & Kind, R. *Geophys. J. Int.* **107,** 117–129 (1991).
23. Whitcomb, J. H. & Anderson, D. L. *J. geophys. Res.* **75,** 5713–5728 (1970).
24. Whitcomb, J. H. *Bull. seism. Soc. Am.* **63,** 133–143 (1973).
25. Husebye, E. S., Haddon, R. A. W. & King, D. W. *J. Geophys.* **43,** 535–543 (1977).
26. Richards, P. G. *Z. geophys.* **38,** 517–527 (1972).
27. Kennett, B. L. N. *IASPEI 1991 Seismological Tables* (Austr. Natn. Univ., Canberra, 1991).
28. Shearer, P. M. *Geophys. J. Int.* (in the press).
29. Cummins, P. R., Kennett, B. L. N., Bowman, J. R. & Bostock, M. G. *Bull. seism. Soc. Am.* **82,** 323–336 (1992).
30. Jones, L. E., Mori, J. & Helmberger, D. V. *J. geophys. Res.* **97,** 8765–8774 (1992).
31. Dziewonski, A. M. & Anderson, D. L. *Phys. Earth planet. Inter.* **25,** 297–356 (1981).

ACKNOWLEDGEMENTS. We thank R. Somera, R. Lester and J. Mori for recovering the P'P' data. T. Wallace provided us with unpublished P'P' results. Discussions with Q. Williams and E. Knittle provided insights into mantle petrology. We acknowledge reviews by R. Engdahl, T. Brocher, T. Lay, J. Revenaugh and P. Shearer. We thank F. Scherbaum and M. Weber for discussions on upper-mantle structure and waveform processing.

Functional topographic mapping of the cortical ribbon in human vision with conventional MRI scanners

Walter Schneider*, Douglas C. Noll*† & Jonathan D. Cohen*‡

* University of Pittsburgh, 3939 O'Hara Street, Pittsburgh, Pennsylvania 15260, USA
† Pittsburgh NMR Institute, 3260 Fifth Avenue, Pittsburgh, Pennsylvania 15213, USA
‡ Department of Psychology, Carnegie Mellon University, Pittsburgh, Pennsylvania 15213, USA

THE human brain has anatomically distinct areas in which processing is laid out in space at the millimetre level with substantial variation across individuals. Activity occurs along a cortical ribbon 1.5–3 mm thick[1] in response to specific stimuli[2,3]. Here we report the first use of cortical ribbon analysis on humans using non-invasive functional magnetic resonance imaging techniques performed with a conventional 1.5 T MRI scanner. Changes in activation were detected using T2*-weighted, gradient echo imaging sequences. Subjects observed partial field, flashing checkerboard patterns (left–right, top–bottom, half rings, and wedges). Stimuli produced magnetic resonance signal changes in the 1–8% range, varying at the millimetre scale, which showed contralateral vertically reflected patterns of activation in the visual cortex. To compare the spatial topographies across subjects, computer algorithms were used to control for the subject-unique folding of cortex, providing a flattened cortical ribbon identifying four topographically distinct areas.

Changes in cortical metabolism and cerebral perfusion have been recorded non-invasively in humans with positron emission tomography (PET)[4], and functional magnetic resonance imaging (FMRI)[5–7], typically with special purpose high-speed imaging devices and/or on high-field MR devices. We used conventional MRI scanners (1.5 T Signa, 4.7 software release; GE Medical Systems, Milwaukee) with standard scanning software and a surface coil centred over the occipital pole. Six normal subjects underwent FMRI imaging. Functional imaging scans used T2*-weighted, gradient echo sequences with late echo times (TE, 40 ms) based on previous FMRI studies[5]. A multiple slice scanning sequence (flip angle, 30 degrees; repetition time, TR, 100–150 ms; in-plane resolution 1.88 × 0.94 mm) was used to produce 2–6 slices (each 6–10 mm in thickness) per trial. There were 10 trials per condition. Each trial included 10 s of stimulation, 28–60 s of stimulation plus scanning (depending on the number of slices recorded), and a 5-s inter-trial interval. The magnetic resonance parameters used for functional scans are thought to be sensitive to levels of blood oxygenation[8]. Signal dephasing occurs at a microscopic (subvoxel) level in tissues surrounding the vessels when haemoglobin becomes deoxygenated[9].

The statistical significance of differences was evaluated using a group t-test[10] for each voxel (0.93 × 0.93 mm volume element) of the image. Owing to the use of a surface coil, the signal magnitude decreased with distance from the pole (reaching 50% at 5 cm). Voxels with less than 50% signal were excluded from the analysis. We used several criteria: to identify the extent (in voxels and mm^2) of activated regions, an α-level of $P<0.05$ (one-tailed $t(\text{d.f.}=18)>1.73$) was used, and to show the reliability of the effect, criteria at the $P<0.005$ and $P<0.0005$ levels are provided. In addition, we statistically defined regions of interest through particle analysis, rejecting voxels that were not part of a contiguous set of at least 16 voxels on sagittals, and 8 on coronals (with either sides or corners touching).

On each trial, the subject was presented with a partial field reversing checkerboard pattern, reversing at a rate of 8 Hz[5,11]. The subject's task was to monitor for rare targets (average 1 per 10 s) of either a brief (50 ms) flash of a white square, or movement of a fixation cross. Stimuli were presented by rear-projecting computer-generated images produced on an active matrix liquid crystal display projection panel. The subject viewed the stimuli through prism glasses on a screen at the subject's feet. The visual angles of the stimulus were 18 deg horizontal and 11 deg vertical.

Figure 1 shows sagittal activation images, with the locations of significant differences between the two conditions illustrated in warm (violet, red, yellow) and cool (dark blue, blue, cyan) colours relating to the display. Large areas of significant activation occurred along the lingual and cuneate gyri and in the superior occipital cortex. The activation pattern maps illustrate contralateral (Fig. 1*a*, *b*) vertically reflected (Fig. 1*c*) activation